Machine learning models for predicting microvascular invasion in hepatocellular carcinoma with three-dimensional whole-lesion ^{18}F-FDG PET radiomics

Hong Yang[#] MD,
Dinghua Pang[#] MD,
Shilai Zhang# MD,
Zhi Yang MD,
Meishe Gan MD,
Linlin Wei MD,
Ning Li MD,
Hongjiao Wei MD,
Guoyou Xiao MD,
Hai Liao MD

[#]*Contributed equally*

Department of Nuclear Medicine, Guangxi Medical University Cancer Hospital, Nanning 530021, Guangxi Zhuang Autonomous Region, China

Keywords: HCC - Microvascular invasion - ^{18}F-FDG PET/CT - Radiomics - Machine learning

Corresponding author:
Hai Liao MD,
Department of Nuclear Medicine, Guangxi Medical University Cancer Hospital, Nanning 530021, Guangxi Zhuang Autonomous Region, China
Tel: 18077024005
42442427@qq.com

Guoyou Xiao MD,
Department of Nuclear Medicine, Guangxi Medical University Cancer Hospital, Nanning 530021, Guangxi Zhuang Autonomous Region, China
Tel: 13807807280
xgy725@aliyun.com

Received:
23 December 2025
Accepted revised:
6 April 2026

Abstract

Objective: To estimate the performance of machine learning models based on preoperative three-dimensional whole-lesion radiomics features for predicting microvascular invasion (MVI) in hepatocellular carcinoma (HCC). **Subjects and Methods:** This retrospective study included 106 individuals who underwent preoperative fluorine-18-fluorodeoxyglucose (^{18}F-FDG) positron emission tomography/computed tomography (PET/CT) and were pathologically diagnosed with HCC at Guangxi Medical University Cancer Hospital between January 2018 and December 2023. Individuals were randomly assigned to training (n=74) and validation (n=32) sets. A total of 2,016 radiomic features were extracted from three-dimensional whole-lesion PET images. Least absolute shrinkage and selection operator regression combined with recursive feature elimination identified the optimal feature subset. Logistic regression (LR), Light Gradient Boosting Machine (LightGBM), and multilayer perceptron (MLP) models were developed. Model performance in the validation set was evaluated using precision, area under the receiver operating characteristic curve (AUC), and F1-score. **Results:** Six key radiomic features were selected. In the validation set, the LR model achieved an AUC of 0.703, precision of 0.750, and F1-score of 0.765; the LightGBM model achieved an AUC of 0.654, precision of 0.688, and F1-score of 0.687; and the MLP model achieved an AUC of 0.629, precision of 0.625, and F1-score of 0.625. **Conclusion:** The LR model demonstrates the best overall performance and shows promise for noninvasive preoperative MVI assessment.

Hell J Nucl Med 2026; 29(1): 16-25 *Epub ahead of print: 7 April 2026* *Published online: 30 April 2026*

Introduction

Hepatocellular carcinoma (HCC) is the sixth most common cancer worldwide and the second leading cause of cancer-related deaths in China, imposing a substantial disease burden [1]. In 2022, China recorded 316,500 deaths from liver cancer [2]. Although surgical resection and liver transplantation remain the primary HCC treatments, postoperative recurrence rates remain high (50%-70%), which considerably impairs long-term survival outcomes [3-5]. Microvascular invasion (MVI), defined as the existence of tumor cell nests within the vascular lumen on microscopic examination, is a key pathological factor contributing to early postoperative HCC recurrence [6]. A large meta-analysis demonstrated that MVI is an independent risk factor for poor prognosis in individuals with HCC. Microvascular invasion resulted in a significantly decreased 5-year overall survival rate (hazard ratio [HR]=2.05, 95% confidence interval [CI]: 1.75-2.40) [7]. Therefore, for patients with MVI confirmed preoperatively or postoperatively, more aggressive surgical strategies such as anatomical liver resection or transplantation are often considered in clinical practice [8].

Currently, conventional imaging techniques have limited accuracy in the preoperative identification of MVI status and rely mainly on postoperative pathological diagnoses. Although preoperative biopsy provides an alternative, it is invasive, limited by significant tumor heterogeneity and sampling constraints, and has a sensitivity of less than 60% [9]. Therefore, clinical practice requires the development of a noninvasive and precise preoperative technique for predicting MVI.

Radiomics, which allows high-throughput isolation of deep quantitative characteristics from medical images, can noninvasively quantify intratumoral heterogeneity, thereby revealing the pathological microenvironment and biological behavior of the tumor and providing an important basis for precision medicine [10, 11]. Recently, several advances have been made in studies based on multimodal imaging for MVI prediction. Specifically, CT-based studies have demonstrated that radiomics models using arterial or portal venous

phase images perform well (AUC=0.73-0.80) [12, 13], although consensus regarding the optimal imaging phase is lacking. MRI-based studies have shown excellent predictive performance for T2-weighted imaging sequences (AUC=0.808) [14]; however, standardized protocols for contrast agent administration and multi-sequence combination strategies are still lacking. Additionally, ultrasound radiomics has shown potential in meta-analyses (pooled AUC=0.81) [15]; however, its results are susceptible to operator experience and equipment variability [16]. More importantly, these morphological imaging modalities are limited in their ability to directly capture the metabolic behavior of tumors.

Fluorine-18-fluorodeoxyglucose (^{18}F-FDG) positron emission tomography/computed tomography (PET/CT) integrates precise anatomical localization with functional metabolic data and provides a unique perspective to overcome the above limitations. Investigations have illustrated that metabolic parameters from ^{18}F-FDG PET/CT metabolic parameters (e.g., metabolic tumor volume [MTV] and total lesion glycolysis [TLG]) are significantly associated with MVI and can serve as noninvasive preoperative predictors [17, 18]. Furthermore, PET radiomic features can reveal metabolic heterogeneity within tumors, offer more comprehensive information for MVI prediction, and demonstrate promise in predicting MVI in HCC [19, 20]. For example, a model based on two-dimensional PET/CT features developed by Wang et al. (2022) achieved an AUC of 0.806 for the validation set [19], whereas an investigation by Li et al. (2021) focusing on early-stage HCC reported an AUC of 0.692 [20]. Nevertheless, these studies have several limitations. First, feature extraction is often limited to two-dimensional slices and does not fully utilize the information on the three-dimensional spatial heterogeneity of tumors. For instance, in the study by Wang et al. (2022), two-dimensional slices covered only approximately 28.7%±6.2% of the tumor volume [19]. Second, model development typically relies on a single machine-learning algorithm, and systematic comparison and validation across different algorithms remain lacking. For example, the single random forest model used by Li et al. (2021) had a cross-validation AUC variation as high as 0.21 [20].

In the present study, a multi-algorithm machine learning framework based on three-dimensional whole-lesion ^{18}F-FDG PET radiomic features was developed to overcome the limitations of traditional two-dimensional radiomic analysis and address the challenges of comprehensive feature extraction and model generalizability. Specifically, a three-dimensional volume of interest (VOI) segmentation strategy was employed, and tumor contours were delineated slice-by-slice to avoid areas of necrosis. The features were then comprehensively extracted from the original images and the eight types of filtered images. Subsequently, the predictive performances of the light gradient boosting machine (LightGBM), logistic regression (LR), and multilayer perceptron (MLP) algorithms were systematically compared, and the optimal model for preoperative MVI prediction was identified. This framework was designed to provide a novel, noninvasive, and accurate approach for preoperative MVI evaluation in patients with HCC, thereby offering imaging-based evidence to support individualized clinical decision-making.

Subjects and Methods

Study Population

The present investigation retrospectively included 106 individuals with HCC who underwent preoperative ^{18}F-FDG PET/CT at Guangxi Medical University Cancer Hospital between January 2018 and December 2023. Among them, 93 were men and 13 were women, and the average age was 52.41±11.44 years.

Inclusion criteria:

1) Postoperative pathological confirmation of HCC with a definitive MVI status. 2) Preoperative ^{18}F-FDG PET/CT images of sufficient quality for radiomic analysis.

Exclusion criteria:

1) Receipt of antitumor therapy such as transcatheter arterial chemoembolization, radiotherapy, or targeted therapy before PET/CT examination. 2) Postoperative pathology indicating combined-type HCC or indeterminate MVI status. All 106 individuals were classified into MVI-positive (n=43) and MVI-negative (n=63) groups according to the postoperative pathological results. The individuals were then randomly assigned in a 7:3 ratio to a training set (n=74) for model creation and validation set (n=32) for performance estimation. This study was approved by the Ethics Committee of Guangxi Medical University Cancer Hospital. Owing to the retrospective nature of the study, informed consent was not required.

Acquisition of ^{18}F-FDG PET/CT image

All images were acquired using a GE Discovery 710 PET/CT scanner. The radiotracer ^{18}F-FDG was produced in-house using an HM-10HC cyclotron (Sumitomo, Japan) and an F300E-2 chemical synthesizer (Sumitomo, Japan). The radiochemical purity was >95%. Individuals fasted for at least 6h before the scan, and their fasting blood glucose levels were <11.1mmol/L. Subsequently, ^{18}F-FDG was administered intravenously at a dose of 3.70-5.55MBq/kg according to body weight. After a 60-min resting period, scanning was performed. Low-dose CT (tube voltage, 120kV; tube current auto modulation) was initially performed for anatomical localization and attenuation correction. Then, PET emission scanning was conducted (3D acquisition mode, 7-8 bed positions, 1.5 min/bed position). Positron emission tomography images were reconstructed using an iterative algorithm, and all images were archived in DICOM format in the PACS system for potential future use. All image analyses were performed independently by two senior nuclear medicine physicians who were blinded to the clinical and pathological information. Any discrepancies were resolved by consensus.

Collection of clinical and imaging variables

1) Clinical variables included age, body mass index (BMI), alcohol use, hepatitis B, alpha-fetoprotein (AFP), sex, glutamate dehydrogenase (GLDH), serum albumin (ALB), aspartate aminotransferase (AST), alanine aminotransferase (ALT), and gamma-glutamyl transferase (GGT).

2) Imaging variables included tumor size (maximum diameter measured on PET/CT fusion images); metabolic parameters acquired using a 40% SUV threshold method; maximum (SUVmax), mean (SUVmean), and peak (SUVpeak) standar-dized uptake values; TLG; and MTV.

Target delineation and feature extraction

Target delineation

Manual delineation of the boundaries of each HCC lesion was performed slice-by-slice on PET/CT fusion images by a nuclear medicine physician blinded to pathological outcomes using ITK-SNAP software (version 3.8). Three-dimensional volumes of interest (VOI) were generated for all lesions. Only the largest lesion was delineated in the individuals with multiple lesions. To ensure reproducibility, images from 30 randomly chosen individuals were redelineated by another physician. All delineations were performed strictly along the edges of the metabolically active tumor regions, and areas of necrosis, cystic changes, and adjacent large vessels were avoided (Figure 1).

Feature extraction

The delineated VOI and corresponding images were imported into Python (version 3.7.10). First, all images were resampled to an isotropic resolution of 3×3×3mm^3 using the nearest-neighbor interpolation method as a preprocessing step. Subsequently, for each patient, features were extracted from the original images and images processed with eight different filters: Laplacian of Gaussian, wavelet transform (Wavelet), square, square root, exponential, gradient, logarithm, and three-dimensional local binary pattern, using PyRadiomics (v. 3.0.1). Seven feature categories were extracted: first-order statistics, neighboring gray-tone difference matrix, shape (3D), gray-level co-occurrence matrix, run-length matrix, gray-level size zone matrix, and gray-level dependence matrix. The initial feature pool included 2,016 features.

Feature selection and model development

Feature selection

A four-step feature selection procedure was employed to eliminate overfitting and multicollinearity:

1) Features with an intraclass correlation coefficient (ICC) ≥ 0.75, which accounted for 82.3% of all features, were retained to ensure inter-observer consistency.
2) The Mann-Whitney U test was initially used to screen features ($P<0.05$). 3) Recursive feature elimination was conducted to address multicollinearity, and low-variance features were removed when $|r|>0.9$.
4) Least absolute shrinkage and selection operator (LASSO) regression with 10-fold cross-validation ($\lambda=0.0146$) was applied to compress the feature space. Ultimately, six features were selected for model development (Figure 2).

Model development and evaluation

The six selected core features were input into three machine learning algorithms (LR, LightGBM, and MLP) to develop predictive models for MVI. All models were trained on the training set, and their performance was assessed using an independent validation set. The performance metrics included precision, area under the receiver operating characteristic (ROC) curve (AUC), and F1-score. The DeLong test was used to compare the AUC of the ROC curves between the different models.

Statistical methods

Continuous variables with normal distributions are expressed as mean±standard deviation $(\bar{x} \pm s)$, and the independent-samples t-test was employed for comparison. Data with non-normal distribution are reported as median (interquartile range) [M (P25, P75)] and were compared using the Mann-Whitney U test. Categorical variables were presented as frequencies (n) and percentages (%), and the chi-square test or Fisher's exact test was used for comparison. Univariate logistic regression was used to assess the associations between the clinical and imaging variables and MVI status. IBM SPSS Statistics (version 26.0) and Python 3.7.10 were utilized for statistical analyses, with significance set at $P<0.05$.

Results

Baseline clinical and imaging characteristics

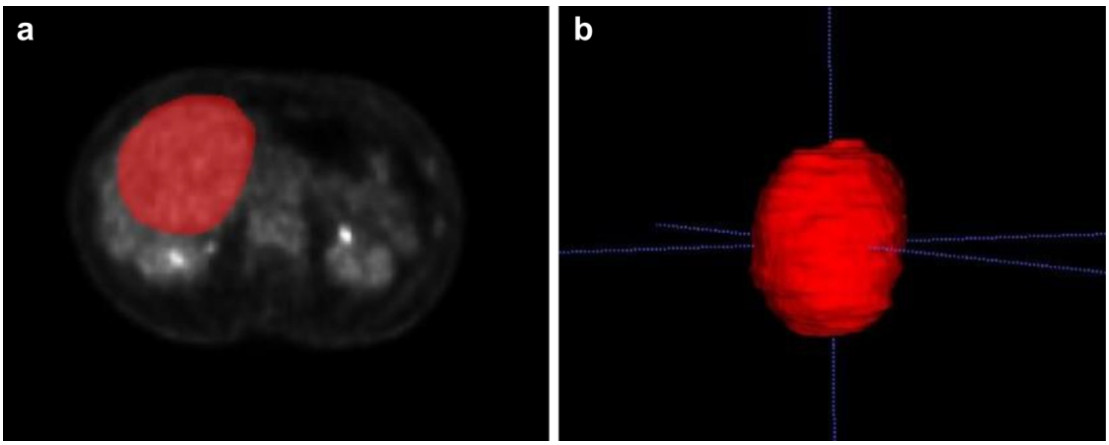

Figure 1. Three-dimensional target delineation and merged VOI generation. Note: A represents manual slice-by-slice region of interest (ROI) delineation, and B represents the volumes of interest (VOI) generated by merging ROI.

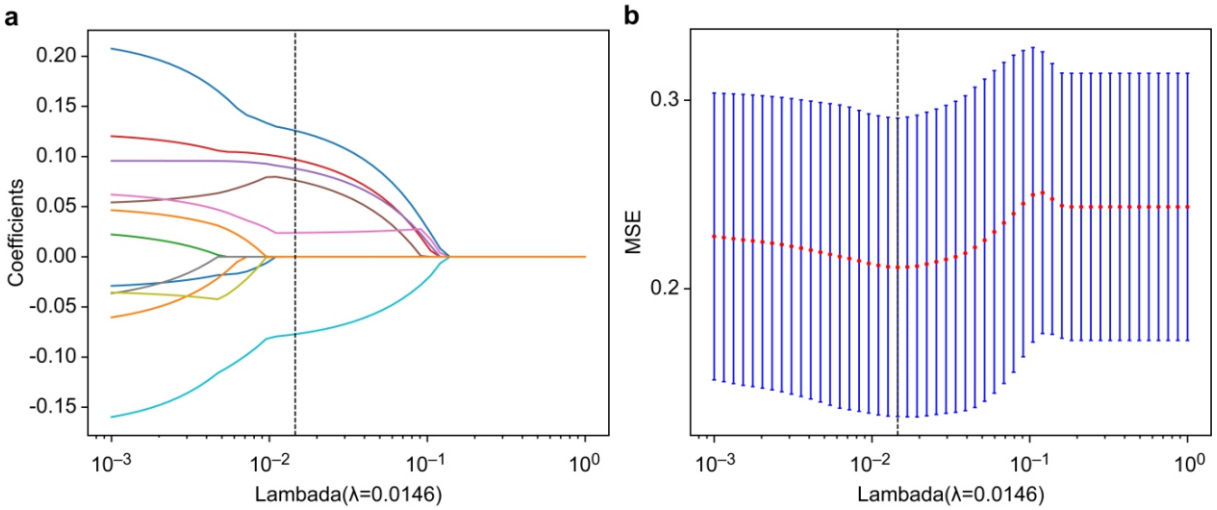

Figure 2. Selection of radiomic features using LASSO regression combined with cross-validation of 10 folds. Note: A. LASSO coefficient profile plot (shows changes in feature coefficients with varying λ);B. Cross-validation plot (the minimum mean square error [MSE] occurs at λ=0.0146) "Coefficients" represent feature coefficients; "MSE" represents mean square error.

The distribution of MVI positivity did not differ significantly between the investigated sets (45.9% vs. 28.1%, P=0.134). The baseline clinical and imaging characteristics between the two sets did not vary significantly with respect to sex, age, BMI, tumor size, or PET metabolic parameters (all P>0.05), except for a history of hepatitis B (P=0.023). This indicates a balanced dataset partitioning. Details are presented in Table 1.

Univariate analysis of clinical and imaging variables associated with MVI status in the training set

Univariate logistic regression analysis was conducted on the training set to estimate the correlation between clinical and conventional imaging variables and MVI status. Among all variables assessed for their association with MVI status, only tumor size was significantly associated with MVI status (OR= 1.149, 95% CI, 1.003-1.316; P=0.046). Sex, age, AFP level, liver function parameters (ALT, AST, GGT, GLDH, and ALB), and PET metabolic parameters did not show significant predictive value (P>0.05). Details are presented in Table 2.

Radiomic feature selection results

A total of 2,016 features were extracted from the original and filtered images. After a four-step selection process, the six non-redundant features most closely associated with MVI were retained for model development. Figure 3 shows the coefficients of these characteristics.

Development and performance evaluation of predictive models

Based on the six selected characteristics, LR, LightGBM, and MLP predictive models were developed. Table 3 shows the performance metrics of each model for the training and independent validation sets, and Figure 4 shows the corresponding ROC curves.

In the validation set, the LR model demonstrated the best overall performance, superior to those of the LightGBM and MLP models (AUC: 0.703 vs. 0.654 vs. 0.629; accuracy: 0.750 vs. 0.688 vs. 0.625; F1-score: 0.765 vs. 0.687 vs. 0.625). De Long's test showed no significant variation in the AUC between the investigated sets for all the models (P>0.05, Table 4). This indicates that overfitting did not occur. Although pairwise comparisons of AUC between models in the validation set did not show significant differences (P>0.05, Table 5), a comprehensive evaluation demonstrated that the LR model had the best and most stable performance (Figure 5).

Discussion

In this study, we developed and compared three machine learning models for preoperative MVI prediction in HCC using 3D whole-lesion ^{18}F-FDG PET radiomics. The primary finding of this study was that the LR model demonstrated the most stable and best overall performance in the independent validation set (AUC: 0.703, precision: 0.750, F1-score: 0.765), offering a reliable and interpretable tool for noninvasive MVI assessment.

Methodological strengths of the present 3D whole-lesion PET radiomics approach

The primary methodological strength of our work lies in the adoption of a 3D whole-lesion radiomics analysis on PET images, a meaningful advancement over prior 2D slice-based approaches which may capture only a fraction of tumor volume and heterogeneity [19]. By delineating the entire tumor volume, our method comprehensively captures spatial heterogeneity, which is crucial for characterizing aggressive biological behaviors such as MVI. Furthermore, the use of ^{18}F-FDG PET imaging offers unique advantages for MVI prediction.

Table 1. *Comparison of baseline characteristics.*

Clinical and imaging variables	Training Set (n=74)	Validating Set (n=32)	P-value
Sex (male/female)	67/7	26/6	0.205
Age (years, x±s)	52.41±11.44	52.75±7.84	0.858
BMI (kg/m², median [P25, P75])	22.62 [20.42, 25.38]	24.41 [20.42, 26.44]	0.327
History of alcohol use (no/yes)	41/33	23/9	0.111
History of hepatitis B (no/yes)	22/52	3/29	0.023
History of cirrhosis (no/yes)	34/40	12/20	0.421
AFP (ng/mL, [P25, P75])	71.55 [6.02, 936.00]	102.45 [8.67, 1200.00]	0.502
ALT (U/L, [P25, P75])	37.00 [26.75, 56.50]	37.50 [20.00, 51.25]	0.506
AST (U/L, [P25, P75])	42.00 [32.75, 61.00]	43.00 [33.25, 51.00]	0.603
GLDH (U/L, [P25, P75])	9.50 [6.00, 13.00]	7.00 [6.25, 10.00]	0.114
GGT (U/L, [P25, P75])	65.50 [40.00, 98.50]	68.50 [47.75, 111.00]	0.570
ALB (g/L, x±s)	37.64±4.68	38.49±3.63	0.362
Tumor size (cm, [P25, P75])	5.25 [3.30, 8.23]	4.90 [3.43, 7.45]	0.931
SUVmax (median [P25, P75])	5.79 [4.22, 7.71]	6.89 [4.41, 9.56]	0.106
SUVmean (median [P25, P75])	3.11[2.50, 4.19]	3.72 [2.60, 5.45]	0.126
SUVpeak (median [P25, P75])	4.30 [3.29, 6.42]	5.17[3.43, 7.46]	0.224
MTV (median [P25, P75])	78.41 [38.19, 231.18]	52.62 [19.23, 121.75]	0.065
TLG (median [P25, P75])	248.30 [129.45, 631.43]	219.40 [75.69, 573.45]	0.203
MVI (negative/positive)	40/34	23/9	0.086

Table 2. *Univariate analysis of clinical and imaging variables linked to MVI status in the training set.*

Clinical and imaging variables	Univariate analysis		
	OR	95% CI	P-value
Gender (male/female, 67/7)	3.276	0.593-18.104	0.174
Age (years, 52.41±11.44)	1.010	0.970-1.051	0.634
BMI (kg/m², 23.02±3.35)	0.987	0.860-1.133	0.854
History of alcohol use (no/yes, 41/33)	0.965	0.385-2.421	0.939
History of hepatitis B (no/yes, 22/52)	0.611	0.224-1.667	0.336
AFP (ng/mL, 71.55 [6.02, 936.00])	1.000	1.000-1.001	0.382
ALT (U/L, 37.00 [26.75, 56.50])	0.998	0.990-1.006	0.624
AST (U/L, 42.00 [32.75, 61.00])	0.999	0.992-1.006	0.777
GLDH (U/L, 9.50 [6.00, 13.00])	1.001	0.970-1.032	0.959
GGT (U/L, 65.5 [40.00, 98.50])	1.002	0.998-1.006	0.360
ALB (g/L, 37.64±4.68)	0.993	0.897-1.099	0.889
Tumor size (cm, 5.25 [3.30, 8.23])	1.149	1.003-1.316	0.046
SUVmax (5.79 [4.22, 7.71])	1.065	0.947-1.197	0.294
SUVmean (3.11 [2.50, 4.19])	1.120	0.895-1.401	0.324
SUVpeak (4.30 [3.29, 6.42])	1.111	0.948-1.302	0.193
MTV (78.41 [38.19, 231.18])	1.003	1.000-1.006	0.102
TLG (248.30 [129.45, 631.43])	1.001	1.000-1.002	0.077

Note: OR=odds ratio.

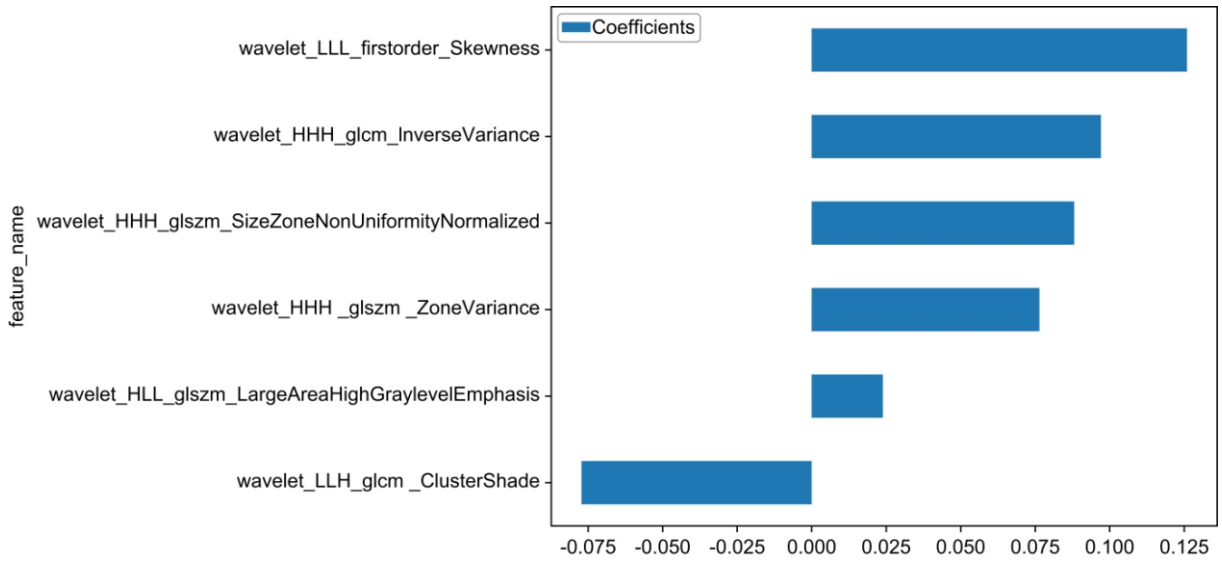

Figure 3. Six key radiomic features selected by LASSO regression and their coefficients. Note: The y-axis denotes the six optimal characteristics, and the x-axis denotes the coefficients.

Table 3. *Performance evaluation of three machine learning models on the investigated sets*

		AUC	Accuracy	F1-score	95% CI	Sensitivity	Specificity
Training set	LR						
		0.808	0.743	0.689	0.697–0.918	0.778	0.723
Validation set		0.703	0.750	0.765	0.508–0.899	0.812	0.687
	Light GBM						
		0.784	0.743	0.642	0.680–0.890	0.630	0.809
		0.654	0.688	0.687	0.455–0.853	0.687	0.687
	MLP						
		0.815	0.716	0.687	0.708–0.921	0.852	0.638
		0.629	0.625	0.625	0.427–0.831	0.625	0.625

Note: The F1-score is a comprehensive metric for binary classification model accuracy. MLP, multilayer perceptron; LR, logistic regression

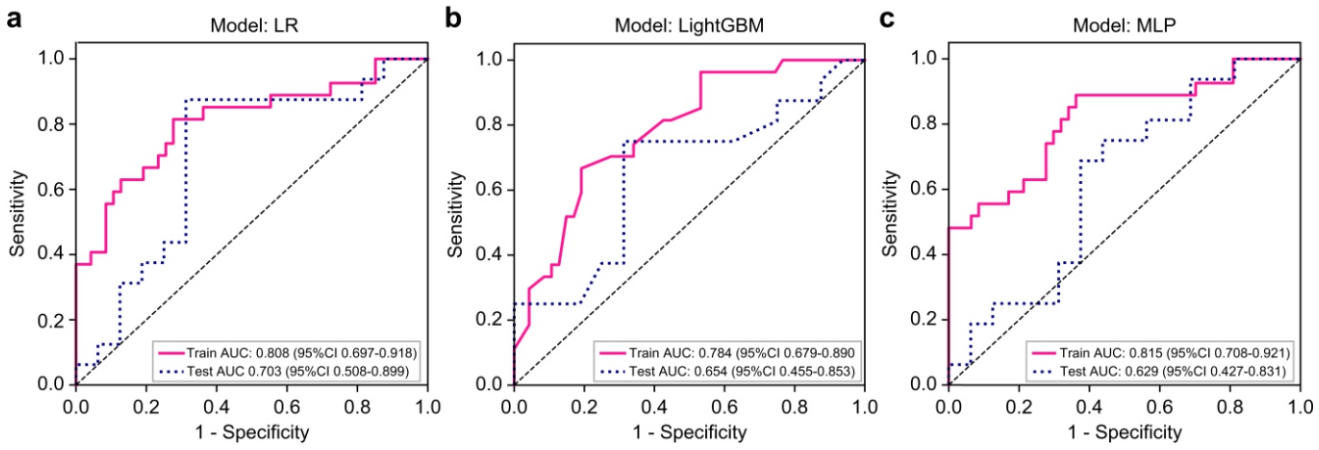

Figure 4. ROC curves of the three machine learning models on the investigated sets. Note: A, B, and C represent the LR, LightGBM, and MLP models, respectively. "Specificity" and "Sensitivity" refer to the respective metrics.

Table 4. *DeLong's test results for AUC comparison between the investigated sets.*

Model (Training set vs. Validation set)	Z value	95% CI	P value
LR	0.929	-0.116–0.325	0.353
LightGBM	1.151	-0.092–0.352	0.250
MLP	1.622	-0.039–0.411	0.105

MLP, multilayer perceptron; LR, logistic regression

Table 5. *DeLong's test results for pairwise AUC comparisons between the three models on the validation set*

Model	Z value	95% CI	P-value
LR vs MLP	-0.417	-0.040–0.026	0.676
LR vs LightGBM	0.446	-0.079–0.125	0.656
MLP vs LightGBM	0.571	-0.074–0.135	0.571

MLP, multilayer perceptron; LR, logistic regression

Unlike conventional anatomical imaging modalities, PET provides functional information about tumor glucose metabolism, which has been shown to correlate with tumor aggressiveness and metastatic potential [21]. The metabolic activity captured by PET may reflect underlying biological processes involved in MVI development, including angiogenesis, hypoxia, and epithelial-mesenchymal transition [22]. In our study, wavelet-derived first-order features and texture features capture the intensity and spatial distribution of metabolic heterogeneity within tumors, which is consistent with the evidence that PET-derived metabolic heterogeneity indicators are significant predictors of MVI [23]. The reproducibility and standardization of our 3D whole-lesion segmentation protocol represent additional strengths. By employing a standardized approach to tumor delineation and feature extraction, we minimize inter-observer variability and enhance the clinical applicability of our method. This is particularly important for multicenter validation and eventual clinical imple-

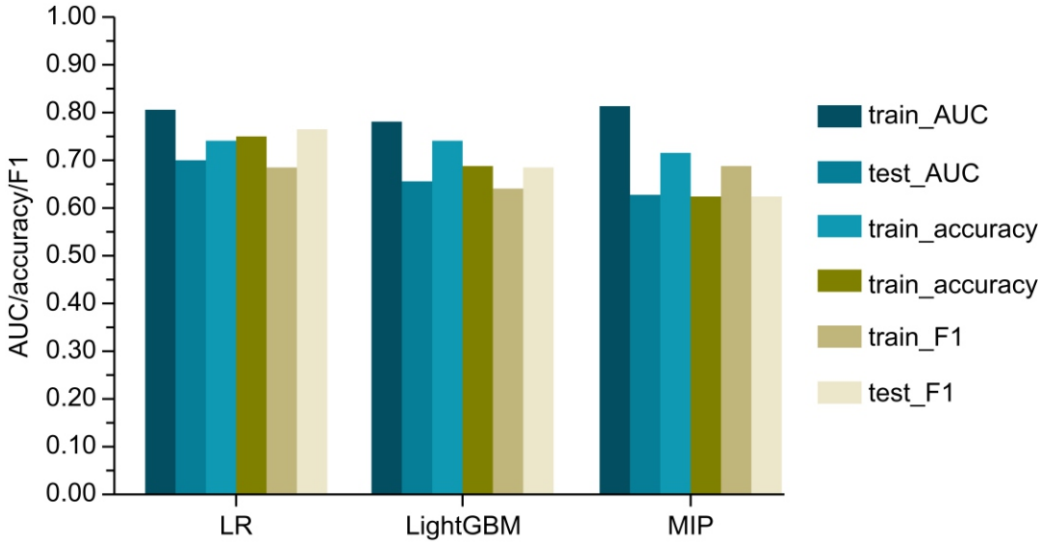

Figure 5. AUC, accuracy, and F1-score of the 3 machine learning models. Note: "Accuracy" refers to accuracy; the x-axis denotes the model type, and the y-axis denotes the metric value.

mentation [24] . The superiority of 3D radiomics is supported by studies showing higher feature stability and predictive performance compared to 2D methods in HCC and other cancers [25, 26].

Interpretability and performance of the logistic regression model

A central finding of our study is that the relatively simple LR model outperformed more complex algorithms (LightGBM and MLP). This can be attributed to several factors well-suited to the context of radiomics with limited sample sizes. First, LR, particularly with regularization, effectively balances feature selection and mitigates overfitting in high-dimensional, small-sample settings, promoting better generalizability [27]. Second, its inherent robustness to noise and lower risk of overfitting compared to complex, high-capacity models like MLP is advantageous when inter-feature correlations are moderate, as in our data [28]. Most importantly, the LR model offers high interpretability by providing explicit feature coefficients (e.g., β=1.86 for Wavelet-LLH_glszm_ ZoneEntropy), translating the "black box" of radiomics into a transparent decision framework [29]. This interpretability is crucial for building clinical trust and facilitating the integration of such models into preoperative decision-making workflows.

Limitations and future directions

This study has numerous limitations. First, as this was a single-center retrospective investigation with a relatively small sample size (n=106), the generalizability of the models may be limited. Second, although tumor size was identified as a significant predictor of MVI (P=0.046), it was not integrated with radiomics features to develop a combined model. Finally, although the reproducibility of manual VOI delineation was ensured by ICC assessment (ICC≥0.75), this process remains subjective.

To address these limitations, we propose the following future research directions: (1) conducting large-scale, multicenter prospective investigations to further confirm model performance, (2) exploring the integration of clinical predictors with predictive value, such as tumor size, with radiomic features to develop multimodal predictive models, and (3) developing automated medical image segmentation systems based on deep learning (e.g., U^2-Net [30]) to improve segmentation efficiency and objectivity.

In conclusion, the LR model developed on the basis of three-dimensional whole-lesion ^{18}F-FDG PET radiomic features demonstrates promising predictive ability for MVI status in HCC and may act as an effective noninvasive tool for MVI preoperative evaluation.

The authors declare that they have no conflicts of interest.

Acknowledgments

We would like to thank Editage (www.editage.com) for English language editing.

Funding

This study was supported by the Open Project of Guangxi Key Laboratory of Biological Targeted Diagnosis and Treatment (grant number: GXSWBX202203; grant recipient: Guoyou Xiao).

Ethics approval

The studies involving humans were approved by Ethics Committee of Guangxi Medical University Cancer Hospital. This study was conducted in accordance with the local legislation and institutional requirements. The ethics committee/institutional review board waived the requirement of written informed consent for participation from the participants or the participants' legal guardians/next of kin because This article is a retrospective clinical study, and relevant ethics do not apply.

Bibliography

1. Cao W, Chen HD, Yu YW et al. Changing profiles of cancer burden worldwide and in China: A secondary analysis of the global cancer statistics 2020. *Chin Med J (Engl)* 2021; 134(7): 783-91.
2. Han B, Zheng R, Zeng H et al. (2024) Cancer incidence and mortality in China, 2022. *J Natl Cancer Cent* 2024; 4(1): 47-53.
3. Siegel RL, Miller KD, Wagle NS, Jemal A. Cancer statistics, 2023. *CA Cancer J Clin* 2023; 73(1): 17-48.
4. Anwanwan D, Singh SK, Singh S et al. Challenges in liver cancer and possible treatment approaches. *Biochim Biophys Acta Rev Cancer* 2020; 1873(1): 188314.
5. Fujiwara N, Friedman SL, Goossens N, Hoshida Y. Risk factors and prevention of hepatocellular carcinoma in the era of precision medicine. *J Hepatol* 2018; 68(3): 526-49.
6. Roayaie S, Blume IN, Thung SN et al. A system of classifying microvascular invasion to predict outcome after resection in patients with hepatocellular carcinoma. *Gastroenterology* 2009; 137(3): 850-5.
7. Wang W, Ding H, Yu J et al. Impact of microvascular invasion on the long-term survival of patients with hepatocellular carcinoma after liver resection: A systematic review and meta-analysis. *Eur J Surg Oncol* 2023; 49(2): 432-41.
8. Zheng J, Chou J, Liu S et al. Preoperative prediction of microvascular invasion in hepatocellular carcinoma using a radiomics nomogram based on gadoxetic acid-enhanced MRI. *J Hepatocell Carcinoma* 2021; 8: 1453-66.
9. Sun J, Xia Y, Shen F, Cheng S, Chinese Association of Liver Cancer of Chinese Medical Doctor Association. Chinese expert consensus on the diagnosis and treatment of hepatocellular carcinoma with microvascular invasion (2024 edition). *Hepatobiliary Surg Nutr* 2025; 14(2): 246-66.
10. Chen L, Wang K, Xu JN et al. A multi-modal fusion framework combining PET radiomics, clinical indicators and deep learning features for preoperative prediction of microvascular invasion in hepatocellular carcinoma. *J Hepatol* 2025; 82(3): 456-68.
11. Cheng SH, Hu G, Zhang SB et al. Machine learning-based radiomics in malignancy prediction of pancreatic cystic lesions: Evidence from cyst fluid multi-omics. *Adv Sci (Weinh)* 2025; 12(20): e2409488.
12. Zhou Y, Liu Z, Zhang X et al. Preoperative CT radiomics for microvascular invasion prediction. *Radiology* 2021; 301(2): 350-9.
13. Xu T, Zhang Z, Mo X et al. Predicting microvascular invasion using CT-based radiomics model. *Radiology* 2023; 307(2): e222729.
14. Nebbial G, Zhang Q, Arakelian D et al. Pre-operative microvascular invasion prediction using MRI radiomics. *J Digit Imaging* 2020; 33(6): 1376-86.
15. Xiao Q, Zhu W, Tang H, Zhou L. Ultrasound radiomics in the prediction of microvascular invasion in hepatocellular carcinoma: A systematic review and meta-analysis. *Heliyon* 2023; 9(6): e16997.
16. Huang Z, Bian H, Liu J et al. The impact of inter-system and inter-operator variability on ultrasound radiomics feature extraction and analysis: A multi-center study. *Ultrasound Med Biol* 2022; 48(11): 2243-55.
17. Wu F, Cao G, Lu J et al. Correlation between ^{18}F-FDG PET/CT metabolic parameters and microvascular invasion before liver transplantation in patients with hepatocellular carcinoma. *Nucl Med Commun* 2024; 45 (12): 1033-8.
18. Jiang C, Ma G, Liu Q, Song S. The value of preoperative ^{18}F-FDG PET metabolic and volumetric parameters in predicting microvascular invasion and postoperative recurrence of hepatocellular carcinoma. *Nucl Med Commun* 2022; 43(1):100–7.
19. Wang Y, Luo S, Jin G et al. Preoperative prediction using ^{18}F-FDG PET/CT. *BMC Med Imaging* 2022; 22(1): 70.
20. Li Y, Zhang Y, Fang Q et al. Radiomics analysis for microvascular invasion prediction. *Eur J Nucl Med Mol Imaging* 2021; 48(12): 4009-24.
21. Zhong X, Long H, Su L et al. Radiomics models for preoperative prediction of microvascular invasion in hepatocellular carcinoma: a systematic review and meta-analysis. *Abdom Radiol (NY)* 2022; 47(6): 2071-88.
22. Lee SW, Jeong SY, Kim SJ. Diagnostic performance of ^{18}F-FDG PET/CT radiomics in predicting microvascular invasion in hepatocellular carcinoma compared to conventional metabolic parameters: a systematic review and meta-analysis. *Ann Nucl Med* 2025; 39(10): 1146-56.
23. Wang J, Kong X, Cao G, Ye S. Correlation study of ^{18}F-FDG PET/CT metabolic parameters, heterogeneity index, and microvascular invasion, and its nomogram potential in predicting microvascular invasion in liver cancer before liver transplantation. *Nucl Med Commun* 2025; 46(10): 939-48.
24. Lv J, Yin H, Yu H, Shi H. The added value of ^{18}F-FDG PET/MRI multimodal imaging in hepatocellular carcinoma for identifying cytokeratin 19 status. *Abdom Radiol (NY)* 2023; 48(7): 2331-9.
25. Dai H, Lu M, Huang B et al. Considerable effects of imaging sequences, feature extraction, feature selection, and classifiers on radiomics-based prediction of microvascular invasion in hepatocellular carcinoma using magnetic resonance imaging. *Quant Imaging Med Surg* 2021; 11(5): 1836-53.
26. Xu L, Yang P, Yen EA et al. A multi-organ cancer study of the classification performance using 2D and 3D image features in radiomics analysis. *Phys Med Biol* 2019; 64(21): 215009.
27. Liu XY, Wu SB, Zeng WQ et al. LogSum + L2 penalized logistic regression model for biomarker selection and cancer classification. *Sci Rep* 2020; 10(1): 22125.
28. Chen R, Paschalidis IC. A robust learning approach for regression models based on distributionally robust optimization. *J Mach Learn Res* 2018; 19(1): 517-64.
29. Lin L, Spreng RL, Seaton KE et al. GeM-LR: Discovering predictive biomarkers for small datasets in vaccine studies. *PLOS Comput Biol* 2024; 20(11): e1012581.
30. Li X, Fang X, Yang G et al. TransU^2-Net: An effective medical image segmentation framework based on transformer and U^2-Net. *IEEE J Transl Eng Health Med* 2023; 11: 441-50.